Soil Use and Management

WILEY | BRITISH SOCIETY OF SOIL SCIENCE

RESEARCH ARTICLE

Assessing Soil Degradation in Agricultural Landscapes of Semi-Arid Tropics Using Proximal and Remote Sensing-Based Diffuse Reflectance Spectroscopy

Israr Majeed[1] | Sourav Roy[1] | Nagarjuna N. Reddy[1] | Nagaraju Budama[1] | A. Venkataradha[1] | K. H. Anantha[1] | P. Niranjan[1] | Ramesh Singh[1] | M. L. Jat[1,2] | Bhabani S. Das[3] | Kaushal K. Garg[1]

[1]International Crops Research Institute for the Semi-Arid Tropics, Patancheru, Telangana, India | [2]Indian Council of Agricultural Research, New Delhi, India | [3]Agricultural and Food Engineering Department, Indian Institute of Technology Kharagpur, Kharagpur, West Bengal, India

Correspondence: Kaushal K. Garg (kaushal.garg@icrisat.org)

Received: 29 April 2025 | **Revised:** 29 April 2025 | **Accepted:** 2 June 2025

Funding: This study was supported by Ground Water Survey and Development Agency.

Keywords: chemometric models | crop yield | soil degradation index

ABSTRACT

Monitoring soil degradation using the soil degradation index (SDI) is a complex process. Typically, multiple soil parameters are measured under laboratory conditions to create such a composite parameter. Because conventional soil testing methods are tedious and time-consuming, frequent monitoring of soil degradation through SDI continues to be a challenging task. With diffuse reflectance spectroscopy (DRS) emerging as a rapid soil testing method, the major objective of this study is to examine the DRS approach for estimating SDIs in a degradation-prone dryland landscape of Maharashtra, India. Accordingly, surface soil samples were collected from 141 locations and 20 different soil parameters were measured in these samples. Six key parameters were identified to formulate the SDI following a minimum dataset (MDS) approach: soil organic carbon content (SOC), soil erodibility index (eMCR), available S, available Mn, the ratio between exchangeable Ca to Mg and silt content. Spectral reflectance data collected under laboratory conditions and those extracted from multispectral imaging data from Sentinel-2 L2A over the visible to infrared (VNIR) region were used to estimate SDIs and its six indicators by calibrating two popular chemometric models: support vector regression (SVR) and feature selection-based partial-least-squares regression ($PLSR_{FS}$). Results showed that the SDI values could be estimated from the laboratory-measured DRS data with the coefficient of determination (R^2) value of 0.81 and root-mean-squared error (RMSE) value of 0.03. Similarly, chemometric models also performed well for the MSI data ($R^2 = 0.52$; RMSE = 0.04). Although the laboratory-based DRS approach provided greater estimation accuracy, low RMSE values associated with the MSI data showed that SDI may be effectively mapped for the entire study area at high spatial resolution (~10 m for Sentinel-2 L2A data). Correlation analyses between mapped SDI and crop yield further showed yield declines with increasing soil degradation for different rainfed crops, while no such trends were observed for the irrigated crops, suggesting that irrigation management in dryland areas may circumvent land degradation challenges.

Abbreviations: DRS, Diffuse reflectance spectroscopy; PLSR, partial-least-squares regression; $PLSR_{FS}$, PLSR with feature selection; SDI, soil degradation index; SVR, support vector regression.

1 | Introduction

Semi-arid tropics are characterised by water scarcity, land degradation and poor agricultural productivity (Garg et al. 2024). Being the primary livelihood source, agriculture provides employment opportunities to about 55%–60% of the population in dryland areas (FAO 2020). Many of the dryland areas show stagnant agricultural productivity because of soil degradation posing a great threat to current and future food securities, particularly in many developing countries (Lal and Stewart 2019). Reversing soil degradation is crucial for achieving sustainable development goals and ensuring the well-being of living systems. Soil degradation represents a soil's declined capacity to operate as an essential living ecosystem for supporting plants, animals and humans (Lal 2015). Because several factors are responsible for soil degradation, its assessment is typically made by compositing different soil physio-chemical and biological indicators into a suitable soil degradation index (SDI) (Awoonor et al. 2024). In general, the conventional wet chemistry-based soil testing methods used for creating such large databases are labour-intensive, time-consuming and often expensive. Moreover, most of these laboratory-based datasets are generated at a coarser scale (point-scale data) with limited options for creating spatially contiguous information systems needed in identifying corrective measures to address soil degradation.

Over the last two decades, diffuse reflectance spectroscopy (DRS) both in the proximal and remote sensing mode of data acquisition has emerged as a powerful tool for evaluating and monitoring soils at different spatial scales (Purushothaman et al. 2024; Zhang et al. 2021; Mzid et al. 2022; Majeed and Das 2024). Specifically, high spectral resolution (~1 nm) proximal sensing data over the visible to shortwave-infrared (VNIR) regions (wavelength: 350–2500 nm) are shown for rapidly estimating several soil properties in the DRS approach (Viscarra Rossel et al. 2022; Meng et al. 2020; Majeed, Garg, et al. 2023). Similarly, remotely sensed hyperspectral (HSR) and multispectral imaging (MSI) data have also been used for estimating multiple soil parameters (Levi et al. 2022; Zhang et al. 2021; Mzid et al. 2022; Majeed, Purushothaman, et al. 2023). Specifically, the high resolution MSI data from the Sentinel 2 (S2) mission from the European Space Agency (ESA) are now increasingly used for estimating soil properties such as soil organic carbon (SOC) contents (Guo et al. 2021; Castaldi et al. 2023), soil texture; (Swain et al. 2021; Mzid et al. 2022), pH (Sun et al. 2025), calcium carbonate ($CaCO_3$; Castaldi 2021), Fe content (de Sousa Mendes et al. 2022), and soil salinity (Wang et al. 2021). Several studies have also shown that the laboratory-based VNIR approach may be used for estimating integrated indices such as soil quality index (SQI) (Gozukara et al. 2022; Majeed et al. 2024; Song et al. 2024). The coefficient of determination (R^2) values exceeded 0.9 in several studies (Gozukara et al. 2022; Majeed et al. 2024). Recently, Majeed and Das (2024) estimated SQIs for a large agricultural catchment (area ~ 2000 km^2) using HSR data collected from the airborne AVIRIS-NG mission. With SDIs inversely proportional to SQIs, the DRS approaches may be effective in mapping soil degradation.

Composite soil indices such as SDIs and SQIs are developed using principal component analysis (PCA) and a suitable compositing algorithm (Leul et al. 2023; Vasu et al. 2024). The key indicator variables are generally chosen as the contributing minimum dataset (MDS) from a larger set of variables using these approaches (Majeed et al. 2024). For example, Awoonor et al. (2024) employed PCA on 23 soil physical and chemical properties to identify sand content, silt-to-clay ratio, SOC contents, exchangeable acidity, CEC, available K and available P as the key SDI indicators. A smaller set of indicator variables (SOC, water-stable aggregates and extractable P) was shown to be adequate in describing the degradation dynamics in the olive farms in Southern Spain (Gómez et al. 2009). Similarly, Adeniyi et al. (2017) selected 22 properties and performed factor analysis to identify clay content, soil organic matter (SOM), CEC and extractable Zn as critical indicators for soil degradation assessment. Recently, Nascimento et al. (2021) have used multitemporal (S2-MSI) images along with climate variables, terrain and soil attributes to develop SDI. These authors combined digital soil mapping, remote sensing and k-means clustering approaches and observed five distinct degradation levels, which correlated well with the SOM contents in their study site. High SOM contents as the sole validation measure for less soil degradation may be limited in areas where SOM is naturally low because of prevailing environmental conditions rather than soil degradation alone, possibly reducing the reliability of SDI predictions in such regions. In general, validation of SDIs using comprehensive soil productivity measures such as crop yield or input utilisation is limited in soil degradation studies. Moreover, reported yield validation studies are generally restricted to point-scale analyses. Limited spatio-temporal analyses of soil degradation preclude understanding SDI's broader impact across different scales, potentially restricting the development of insights into farm-scale degradation trends. Broadening the validation framework to include yield data at larger spatial scales could enhance the robustness of SDI assessments, making them more applicable for practical decision-making in agricultural management.

Assessment of the DRS approach as a rapid proximal sensing method of evaluating soil degradation in agricultural dryland systems and its upscaling through the use of a suitable remote sensing data product would enable land managers to reverse soil degradation while maintaining yield targets. Specifically, the availability of S2 MSI data opens new opportunities to estimate SDI for large geographical areas with high spatial and temporal resolution. Despite the potential of these methods, limited DRS-based studies have been conducted to quantify SDIs, particularly for dryland ecosystems with inherently low SOC containing agricultural landscapes. Thus, this study aimed to evaluate the DRS approach both in the proximal and multispectral remote sensing mode for assessing soil degradation across the dryland landscape of the Deccan Plateau of Central India. Specific objectives of this study are to (i) identify the minimum dataset (MDS) for developing SDI using multivariate methods; (ii) quantify soil properties selected in MDS and SDI using DRS in the proximal and remote sensing mode and (iii) map the soil degradation within agricultural landscapes and validate it with the crop yields.

2 | Materials and Methods

2.1 | Study Area and Soil Sampling

The study area (17°40′17.47″ N, 75°54′37.58″ E) is located near the Bhend village in the southeast fringe of the Indian state of Maharashtra at Deccan plateau (Figure 1) having total geographical area of 1755 ha. This region experiences a semi-arid climate

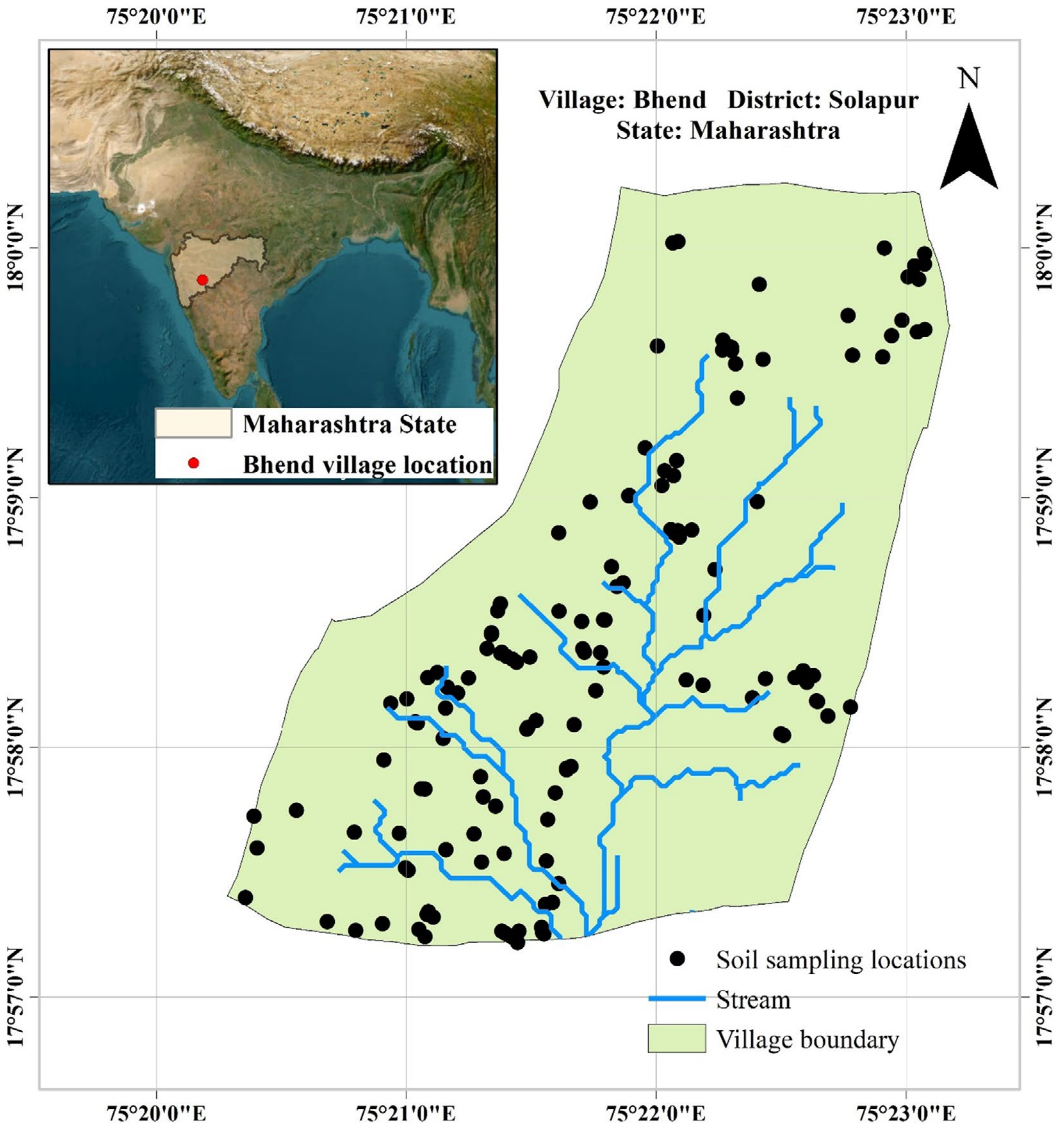

FIGURE 1 | Study area showing the soil sampling locations.

characterised by erratic rainfall and falls under Group B according to the Köppen climate classification with an average annual maximum temperature of 40.1°C and a minimum of 16.1°C. The average annual rainfall is about 650 mm with an average of 20 rainy days in a year. About 40% of annual rain is received during the month of September alone. Agriculture is the predominant land use in the study area, and it serves as the primary source of livelihood for the population. Farmers follow a diverse cropping system and cultivate both during the monsoon (June–Oct.) and post-monsoon season (Nov.–April). Major crops cultivated during the monsoon are black gram (*Vigna mungo*), pigeon pea (*Cajanas cajan*), onion (*Allium cepa*), maize (*Zea mays*), sorghum (*Sorghum bicolor*) and chickpea (*Cicer arietinum*); wheat (*Triticum aestivum*) is grown during the post-monsoon season. Soils of the study area are shallow and have developed from predominantly basaltic rock formations. Groundwater is one of the sources of supplemental irrigation (Birajdar and Shaikh 2024).

To understand the land use dynamics of the study area, a temporal analysis was conducted using Dynamic World land use/land cover maps from 2016 to 2023 (Figure 2). Historically, the study area was characterised by mixed land use with patches of shrublands, tree cover and grasslands. The map depicted major shift in land use patterns including consistent expansion of croplands, with a decline in shrubs, grasslands and tree cover over the years. Moreover, the built-up areas have also increased, particularly in the central and southern region of the study area. Such changes in land use from natural vegetation to intensive croplands often lead to gradual reduction in soil organic matter, cation exchange capacity (CEC) and other essential soil nutrients (Dalal and Jayaraman 2025). The intensification of cropland use, often associated with conventional agricultural practices further accelerates these losses. Hence, leading to systematic degradation of soil health, affecting agricultural productivity and the resilience of agroecological system (Delelegn et al. 2017).

A total of 141 surface soil samples (0–15 cm depth) were collected during June–July 2023 following a random sampling method. Sampling was conducted at field level, where each sample represented a composite of subsamples collected from different points within a single agricultural plot. Collected samples were air-dried, ground and passed through a 2 mm sieve.

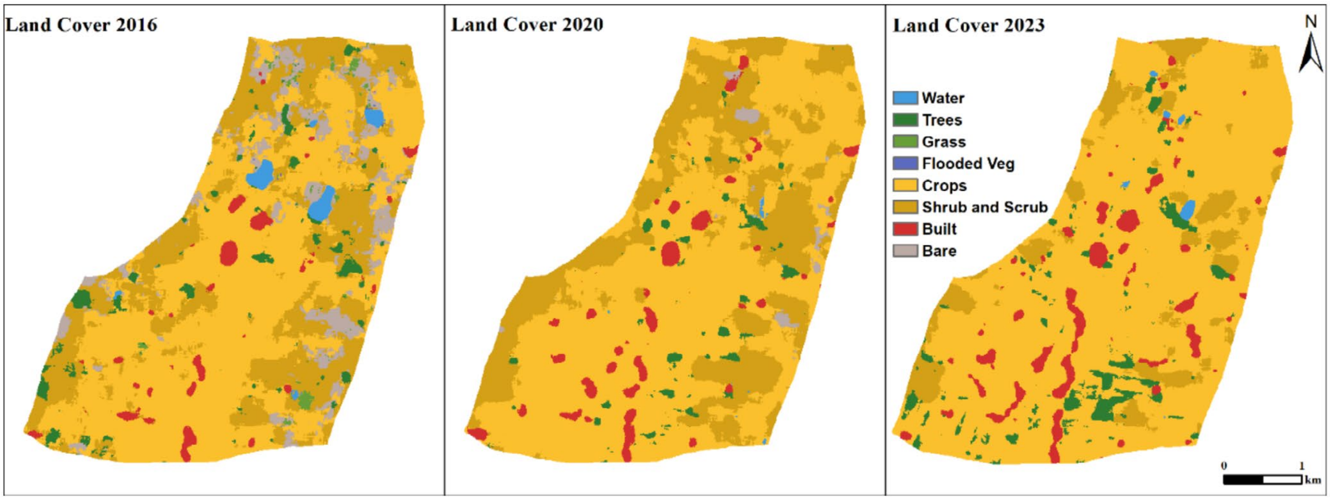

FIGURE 2 | Temporal land use changes from 2016 to 2023 under the study area on the basis of Dynamic World land use/land cover maps.

Each sample was analysed to estimate soil texture (sand, silt and clay), water contents at field capacity (FC) and permanent wilting point (PWP), SOC contents and selected micro-and macro-nutrients. Soil texture was analysed using the hydrometer method (Gee et al. 1986). FC and PWP were determined at −0.33 bar and −15 bar, respectively, using a pressure plate apparatus (Klute 1986). The available water content (AWC) was calculated as the difference between FC and PWP. The chromic acid digestion method (Walkley and Black 1934) was followed to estimate SOC; pH and EC were measured in 1:2 and 1:2.5 soil: water slurry, respectively. Available P was estimated using the Olsen's and Bray's method using a continuous auto-analyser (Olsen and Sommers 1982).

The ammonium acetate method was used to extract available cations such as Ca, Mg, Na and K (Hanway and Heidel 1952). Available B was estimated using the hot water-soluble extraction method (Keren 1996). The diethylenetriamine penta-acetic acid (DTPA) extraction method was used to extract selected micronutrients (Fe, Mn, Cu and Zn) using an inductively coupled plasma (ICP). Along with soil parameters, soil-derived indices such as soil structural stability index (SSSI), soil erodibility index (eMCR) and critical level of SOM (CLOM) were also computed (Tarafdar and Ray 2005; Olaniya et al. 2020; Awoonor et al. 2024); using soil physical properties and SOC:

$$\mathrm{SSSI} = \frac{1.724\,\mathrm{SOC}(\%)}{\mathrm{Clay}(\%) + \mathrm{Silt}(\%)} \times 100 \tag{1}$$

$$\mathrm{eMCR} = \frac{\mathrm{Sand}\,(\%) + \mathrm{Silt}(\%)}{\mathrm{Clay}(\%) + \mathrm{SOC}(\%)} \tag{2}$$

$$\mathrm{CLOM} = \frac{\mathrm{SOM}}{\mathrm{Clay}(\%) + \mathrm{Silt}(\%)} \tag{3}$$

2.2 | Collection of Laboratory VIS–NIR Spectra

Spectral reflectance for each processed soil sample was measured in the laboratory in proximal mode over the VNIR region using a portable spectroradiometer (Model: Field spec4 Hi-Res NG; Malvern Panalytical, UK). A turntable equipped with a halogen bulb was utilised to collect soil spectral data. As indicated in Majeed, Garg, et al. 2023, approximately 100 g of soil sample was placed in a glass petri dish and the soil surface was carefully levelled with a thin glass plate. To calibrate the spectroradiometer and capture reference spectra, the Spectralon white reference panel (Lab sphere, USA) was employed. Soil spectra were collected following the protocol of: (a) warming up the instrument for an hour before data acquisition, (b) performing optimization and reference spectrum collection after every 30 samples and (c) averaging 30 scans per sample. Smoothing of individual spectra was done by a third-order Savitzky–Golay smoothing method with a span length of 9 nm (Savitzky and Golay 1964).

2.3 | Collection and Pre-Processing of Multispectral Data

Sentinel- 2 L2A cloud-free (% cloud cover $\leq$ 5.0%) data were downloaded from the Copernicus Data Space Ecosystem of European space agency. One Sentinel- 2 L2A image covered the entire study area. The downloaded image was pre-processed using SNAP toolbox version 10.0 (https://step.esa.int/main/). Sentinel-2 L2A imagery offers 13 spectral bands at varying spatial resolutions. For this study, nine bands (B2, B3, B4, B5, B6, B7, B8, B11 and B12) were selected on the basis of their relevance in soil applications (Castaldi et al. 2019; Dvorakova et al. 2023). Bands B1, B9 and B10 were excluded because of their primary function in atmospheric correction and cloud detection. To achieve uniform spatial resolution, the Sentinel-2 L2A was resampled to 10 m spatial resolution. To minimise spatial resolution mismatch, Sentinel-2 L2A reflectance data were extracted from the central pixel of each sampling plot, under the assumption that this location is less affected by edge effects and more likely to reflect homogeneous conditions within the field. Moreover, the average field plot size in the study area exceeded the Sentinel-2 L2A pixel resolution (10 m), thereby reducing the risk of mixed-pixel effects. The normalised difference vegetation index (NDVI) was then calculated (Equation 4). The pixels with NDVI values greater than 0.25 were discarded from rest of the analysis to

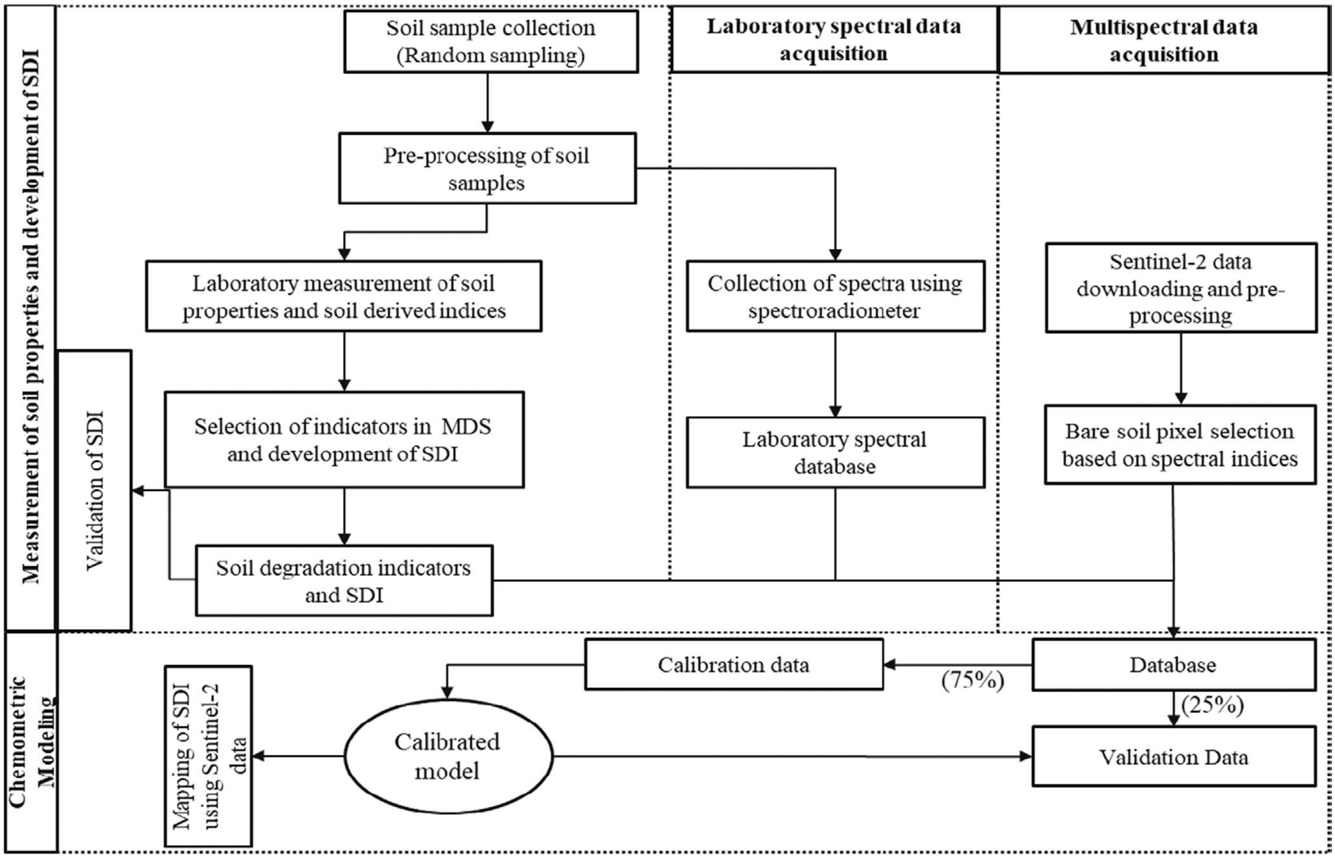

FIGURE 3 | Schematic overview of the framework employed for estimating SDI.

consider only bare soil pixels. Processed spectral reflectance data were then used for chemometric modelling.

$$\mathrm{NDVI} = \frac{(\mathrm{NIR} - \mathrm{RED})}{(\mathrm{NIR} + \mathrm{RED})} \tag{4}$$

where NIR (near-infrared): Band 8 (wavelength: 842 nm) and RED: Band 4 (wavelength: 665 nm).

2.4 | Collection of Primary Data

Primary data was gathered directly from each farmer's field through a structured, in-person interview. This on-site survey was designed to capture an extensive range of data to understand the unique characteristics and management practices for each farm. The survey included farmers' demographic information, specific farm characteristics, crop yields and essential agricultural practices each farmer followed. Detailed data was collected on cropping patterns, types and quantities of fertiliser inputs, cost of cultivation and crop-specific yields. Additionally, the irrigation source along with farm management practices, labour inputs and the use of mechanisation data were also collected.

2.5 | Estimation of the Soil Degradation Index

Figure 3 shows the schematic overview of the methodology adopted to estimate SDI. A total of 20 indicators were selected for soil degradation assessment following PCA. To minimise the number of components, the eigenvalue criterion was utilised (Andrews et al. 2002; Majeed, Garg, et al. 2023; Majeed and Das 2024); components with eigenvalue ≥1 were selected to constitute the MDS (Kaiser 1960). Component loadings assigned to variables under a specific principal component (PC) were utilised to reduce the number of variables. Under each PC, variables within 10% of the highest component loading were selected (Andrews et al. 2002). Pearson correlation coefficients (r) were estimated to remove redundant variables. Among well-correlated variables (i.e., variables with $r > 0.70$), only the variable with the highest factor loading (absolute value) was kept in the MDS (Andrews and Carroll 2001; Andrews et al. 2002). All the selected parameters in MDS were transformed to unitless scores between 0 and 1 using the linear scoring method (more is better, less is better and optimum is better). For the "less is better" function, S_{lin} was estimated by taking the ratio between the minimum value of the indicator variable (X_{min}) and X. For the "optimum is better" function, S_{lin} was estimated by combining both these cases:

$$S_{\mathrm{lin}} = \begin{cases} X/X_{\mathrm{max}}, X < X_{\mathrm{opt}} \\ X_{\mathrm{min}}/X, X > X_{\mathrm{opt}} \end{cases} \tag{5}$$

where X_{opt} denotes the optimum threshold value for X. The MDS values were transformed into degradation score (DS) using Equation (5) below:

$$\mathrm{DS} = 1 - S_{\mathrm{lin}} \tag{6}$$

where S_{lin} is the linear score (between 0 and 1) of a soil variable, X is the magnitude of each soil variable. A score of 0 indicates a complete absence of degradation and 1 indicates the highest SD for the respective soil property (Gómez et al. 2009). The scores were combined into an index (SDI) by applying the weighted additive method (Equation 7):

$$\mathrm{SDI} = \sum_{k=1}^{K} w_k \cdot S_k \tag{7}$$

where w_k and S_k are the kth weight and score of the individual parameter, respectively, and K is the number of soil indicators in the MDS. SDI values were categorised using z-scores: < -1 as low, -1 to 1 as moderate, and > 1 as high degradation (Awoonor et al. 2024). Table 1 shows a benchmarking of the SDI against the SQI on the basis of their respective classification thresholds.

2.6 | Pre-Processing of Spectra and Estimation of Soil Degradation Indicators and SDI

Before carrying out the modelling work, the spectra were pre-processed using first derivative (FD), log-transformed absorbance [log(A)] and SNV (standard variate normal). Following pre-processing, support vector regression (SVR) and modified PLSR models such as $\mathrm{PLSR_{FS}}$ (Sarathjith et al. 2016) were used to estimate soil indicators in MDS as well as SDI. In the SVR approach, training samples are mapped to maximise the width between the observed and predicted responses (Smola and Schölkopf 2004). For the $\mathrm{PLSR_{FS}}$ approach, soil properties are estimated in the PLSR approach after selecting important feature variables (Teofilo et al. 2009; Sarathjith et al. 2016). For this study, 35 predictor variables were considered consisting of PLSR regression coefficients (β), variable influence on projection (VIP), AMI (Sarathjith et al. 2014) and their combinations (Sarathjith et al. 2016). The ordered predictor selection (OPS) approach (Teofilo et al. 2009) was used to identify a parsimonious set of predictors in the algorithm.

The normality of each property was assessed using a two-tailed Kolmogorov–Smirnov test at the 5% significance level.

TABLE 1 | Comparative benchmarking of the soil degradation index (SDI) and the soil quality index (SQI) on the basis of their respective rating scales.

Soil degradation index (this study)		Soil quality index (Qi et al. 2009)	
Range (z score)	**Degradation rating**	**Range**	**Soil quality rating**
< -1	Low	> 0.85	Very High
-1 to 1	Moderate	0.7–0.85	High
> 1	High	0.55–0.7	Moderate
		0.40–0.55	Low
		< 0.4	Very Low

In our study, we considered an observed data point to be an outlier when our chemometric model produced its corresponding estimated value such that the resulting residual (the difference between the observed property and the estimated property) falls outside the 95% confidence interval for all the residuals. The *rcoplot* function in MATLAB can be directly used to identify such outliers (Santra et al. 2009). Specifically, an observation is said to be a potential outlier if the residual error bars did not intersect the zero line in the *rcoplot*, indicating that the predicted value significantly deviated from the observed value. To divide the dataset, a partition sorting approach (Viscarra Rossel et al. 2006) was used, allocating 75% of the data for calibration and 25% for validation. To select calibration and validation subsets, the data were first sorted in ascending order, and every fourth observation was assigned to the validation set (Viscarra Rossel and Lark 2009). This approach ensures that the calibration data and the validation subsets are similar with respect to their general distributions. Statistical similarity between sets was confirmed using two-parameter t-tests (means) and F-tests (variances) at the 5% significance level. All the modelling work was performed using MATLAB R2024a (The MathWorks Inc. 2021, Natick, MA, USA). The prediction performance of the DRS algorithms was assessed using root-mean-squared error (RMSE) and coefficient of determination (R^2):

$$\mathrm{RMSE} = \sqrt{\frac{1}{N}\sum_{i=1}^{N}\left(Y_i - \hat{Y}_i\right)^2} \tag{8}$$

$$R^2 = 1 - \frac{\sum_{i=1}^{n}\left(Y_i - \hat{Y}_i\right)^2}{\sum_{i=1}^{n}\left(Y_i - \overline{Y}_i\right)^2} \tag{9}$$

where Y_i is the measured soil parameter with its mean value of $\overline{Y}_i$ and predicted value of $\hat{Y}_i$ at the ith location and N is the number of locations. All the transformed variables were back transformed before evaluating the performance statistics. For each of these test cases, the best chemometric model and the best transformation of spectra and individual analytes were selected on the basis of the R^2, RMSE and RPIQ values.

A pixel-based predictive modelling approach was used to generate an SDI map for our study area. Specifically, the best-performing chemometric model for SDI was used to convert spectral reflectance data for each pixel of the Sentinel-2 L2A imagery to corresponding SDI values. Pixel-wise SDI values were aggregated to produce a spatially continuous SDI map for the whole study area, effectively capturing variability across the landscape.

3 | Results

3.1 | Descriptive Statistics of Soil Parameters in the Study Area

Table 2 lists the descriptive statistics for measured and estimated soil properties for the soil samples collected from the study area. Despite the small size of the study area, four distinct soil textural classes (clay, clay loam, sandy clay loam and sandy loam) were observed from the measured textural fractions. Soil pH ranged

TABLE 2 | Descriptive statistics of the measured and derived soil parameters.

Soil indicators	Min	Max	Mean	CV	Skewness	Kurtosis
Sand, %	15	84	54	26	−0.37	−0.31
Clay, %	3	67	26	45	0.59	0.16
Silt, %	9	34	19	26	0.43	0.32
FC, g/g	0.09	0.65	0.29	30	1.00	3.34
PWP, g/g	0.05	0.35	0.18	34	0.43	−0.13
AWC, g/g	0.01	0.47	0.10	61	2.05	9.47
Si: CL	0.21	3.50	0.91	58	2.51	8.75
pH	7.37	8.91	8.09	3	0.18	0.45
EC, dS m^{-1}	0.08	3.76	0.51	97	3.04	13.75
SOC, %	0.09	1.19	0.49	41	0.95	0.99
Av. P, mg kg^{-1}	0.17	92.48	11.42	107	3.06	14.79
Ex. K, mg kg^{-1}	4.54	854	82.39	107	5.32	42.22
Av. S, mg kg^{-1}	2.77	438	49.89	114	3.63	18.57
Av. Zn, mg kg^{-1}	0.08	8.82	0.61	145	6.55	55.82
Av. B, mg kg^{-1}	0.20	2.98	0.81	56	1.63	3.95
Av. Fe, mg kg^{-1}	1.32	10.32	4.07	45	0.91	0.69
Av. Cu, mg kg^{-1}	0.86	4.86	2.52	28	0.37	0.04
Av. Mn, mg kg^{-1}	1.46	25.64	6.42	64	1.71	3.62
Ca: Mg	3.04	18.32	5.69	37	3.04	13.55
eMCR[a]	0.48	24.79	3.78	82	3.38	17.13
CLOM[a]	0.002	0.06	0.02	49	1.48	3.09
SSSI[a]	0.27	6.09	2.00	49	1.48	3.09

Abbreviations: Av., available; CLOM, critical level of SOM; eMCR, soil erodibility index; SOC, soil organic carbon; SSSI, soil structural stability index.
[a]Derived soil parameters.

from 7.37 to 8.91 with a mean value of 8.09. This range is typical for soils in arid and semi-arid regions, where low rainfall and high evaporation rates lead to the accumulation of alkaline salts (Bhattacharyya et al. 2013). Electrical conductivity (EC) values varied between 0.08 and 3.76 dS m^{-1}, suggesting the absence of salinity in the region. The average SOC content in the study area was 0.49% with a minimum value of 0.09% and a maximum value of 1.195; 52% of the collected soil samples showed SOC deficiency for the study area. This is likely due to the low organic matter inputs and high mineralization rates in the warm climate of the study area (Lal 2004). In terms of available nutrients, no deficiencies were observed for available Mg, Cu and Mn contents. These nutrients are typically abundant in soils derived from basaltic parent materials, which are common in the Deccan Plateau region (Deshpande et al. 1981). However, the results showed certain deficiencies in specific soil properties. For instance, available P, K, S, Zn, B, Ca and Fe showed deficiencies in 67%, 34%, 46%, 86%, 65%, 8% and 12% of the samples, respectively. These deficiencies can be attributed to various factors such as soil pH affecting nutrient availability and leaching losses (Havlin et al. 1999; Brady and Weil 2008; Majeed, Garg, et al. 2023).

3.2 | Soil Degradation Index

We incorporated physical, chemical and biological properties to create a comprehensive SDI. The SOC was used as a proxy for the biological characteristics (Majeed and Das 2024). From 20 measured soil properties across 141 sampling locations, the PCA results revealed that six PCs had eigenvalues ≥ 1, capturing 77% of the total variability in the dataset (Table 3). The component loading matrix indicated that SOC was the only highly weighted variable in PC1, explaining 27% of the total variance, thus selected for the MDS. The PC2 (20% of variance) revealed that clay contents, the Si:CL ratio and eMCR are the highly weighted variables. With $r > 0.7$ among these three variables (Figure 4), available eMCR was selected for the MDS because of its highest factor loading. For PC3 (12% of variance), EC and available S were the highly weighted variables. On the basis of the correlation coefficient, only available S was retained in the MDS. For PC4 (7% of variance), PC5 (6% of variance) and PC6 (5% of variance), available Mn, Ca:Mg and silt content were the highly weighted variables, respectively, and were included in the MDS. Thus, the MDS consisted of SOC content, eMCR, available S, available Mn, Ca:Mg and silt content. The corresponding weights (Table 3) and

TABLE 3 | Principal component (PC) analysis results and factor loadings for soil indicators.

Principal components	P1	P2	P3	P4	P5	P6
Eigen values	5.71	4.29	2.46	1.41	1.24	1.06
% Variance	27.21	20.43	11.70	6.70	5.90	5.03
% Cumulative variance	27	48	59	66	72	77
Weights	0.353	0.265	0.152	0.087	0.077	0.066
Soil indicators			**Factor loading**			
Sand, %	0.001	0.808	0.049	0.029	0.088	0.531
Clay, %	0.013	**0.893**	0.049	0.005	0.035	0.265
Silt, %	0.030	0.184	0.023	0.071	0.169	<u>**0.886**</u>
AWC, g/g	0.141	0.044	0.285	0.443	0.421	0.272
Si: CL	0.114	**0.924**	0.006	0.022	0.038	0.275
pH	0.281	0.109	0.465	0.505	0.091	0.238
EC, dS m^{-1}	0.136	0.019	**0.919**	0.100	0.130	0.019
SOC, %	<u>**0.916**</u>	0.132	0.235	0.135	0.025	0.147
Av. P, mg kg^{-1}	0.528	0.080	0.087	0.472	0.116	0.041
Ex. K, mg kg^{-1}	0.321	0.114	0.088	0.425	0.114	0.008
Av. S, mg kg^{-1}	0.105	0.001	<u>**0.932**</u>	0.123	0.067	0.018
Av. Zn, mg kg^{-1}	0.543	0.122	0.044	0.266	0.138	0.006
Av. B, mg kg^{-1}	0.504	0.192	0.617	0.070	0.178	0.143
Av. Fe, mg kg^{-1}	0.286	0.036	0.456	0.568	0.429	0.049
Av. Cu, mg kg^{-1}	0.243	0.254	0.012	0.461	0.639	0.074
Av. Mn, mg kg^{-1}	0.213	0.040	0.203	<u>**0.745**</u>	0.071	0.140
Ca: Mg	0.109	0.048	0.125	0.025	<u>**0.788**</u>	0.192
CLOM[a]	0.799	0.510	0.135	0.092	0.010	0.163
eMCR[a]	0.056	<u>**0.935**</u>	0.034	0.061	0.040	0.059
SSSI[a]	0.799	0.510	0.135	0.092	0.010	0.163

Abbreviations: Av., available; CLOM, critical level of SOM; eMCR, soil erodibility index; SOC, Soil organic carbon; SSSI, soil structural stability index.
[a]Bold face underlined factor loadings indicate selected soil properties retained in the minimum dataset (MDS).

these indicators were combined using Equation (7) to yield an expression for the SDI:

$$\begin{aligned} \mathrm{SDI} = {} & 0.353\left(S_{\mathrm{SOC}}\right)+0.265S_{\mathrm{eMCR}}+0.152S_{S}+0.087S_{\mathrm{Mn}} \\ & +0.077S_{\mathrm{Ca:Mg}}+0.066S_{\mathrm{silt}} \end{aligned} \tag{10}$$

The SOC has the largest contribution (35.3%) standing out as the primary contributor to SDI (Figure 5a), followed by eMCR (26.5%). Three other key SDI indicators available S, Mn and Ca:Mg collectively contributed 31.6% to SDI (Figure 5a). The textural component silt played a small yet significant role, contributing 6.6% to the SDI computation. Although an eigenvalue threshold of 1 guided the PC selection, all the textural components were included in the derived parameter eMCR. Figure 5b shows the histogram and kernel density plots of computed SDI values indicating a slightly right-skewed distribution. Resulting SDI values ranged from 0.37 to 0.77 with an average value of 0.60. Figure 6 shows the Q-Q plots for all the indicators selected in MDS. The Q-Q plots reveal that none of these indicators follow a normal distribution, as evidenced by significant deviations from the reference line, especially at higher quantiles.

3.3 | Soil Degradation and Its Interaction With Key Soil Metrics

3.3.1 | Soil Degradation and SOC Content

Figure 7 shows the interaction between soil degradation and SOC content. The SDI values were grouped into three classes using the z value of each score and categorised as follows: scores between −1 and 1 were classified as moderate degradation, scores greater than 1 as high degradation and scores less than −1 as low degradation (Awoonor et al. 2024). There

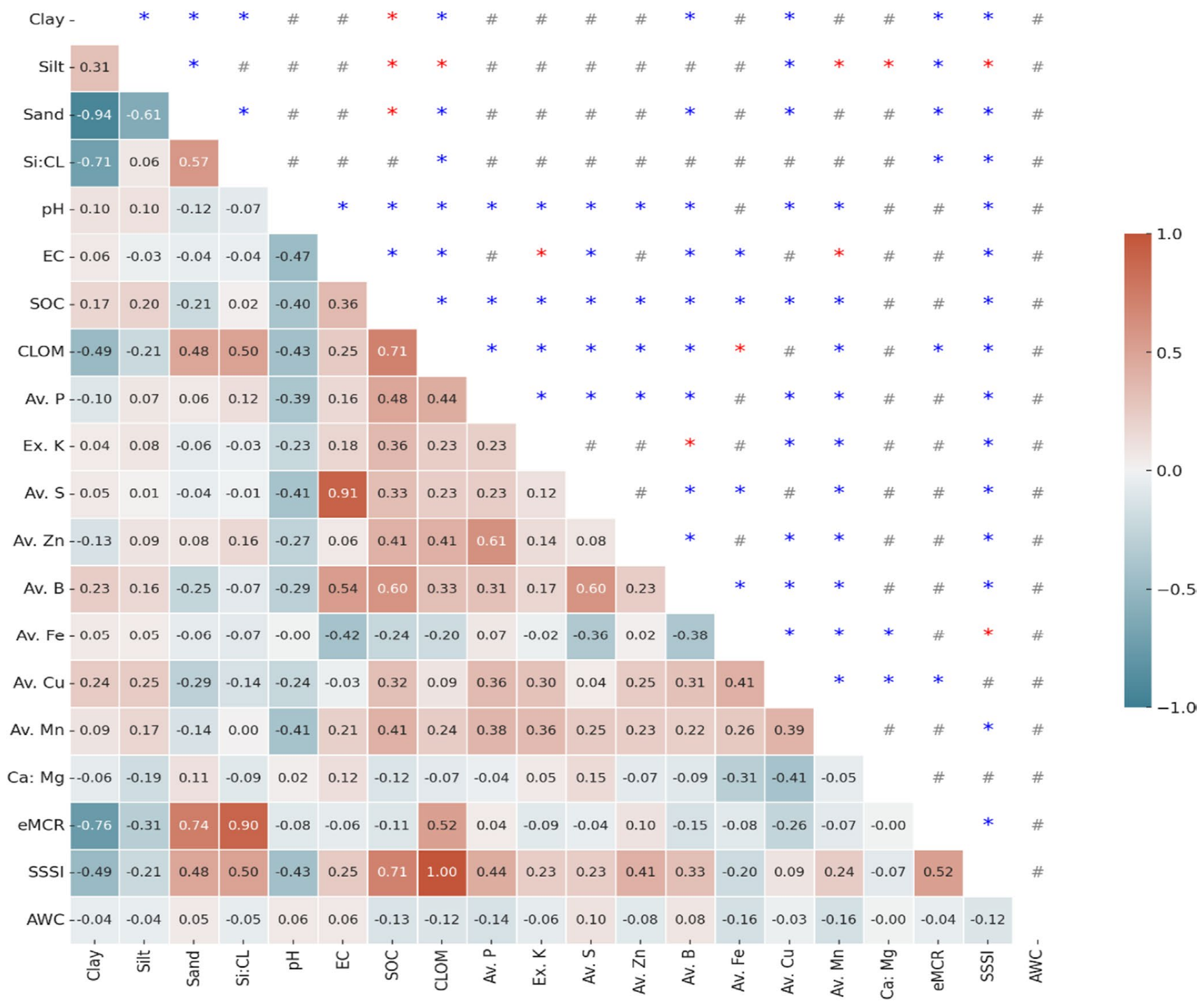

FIGURE 4 | Heat map showing the correlation among soil Indicators. Blue asterisk (*) for correlations significant at the 1% level; red asterisk (*) for correlations significant at the 5% level. Hash symbol (#) for non-significant correlations.

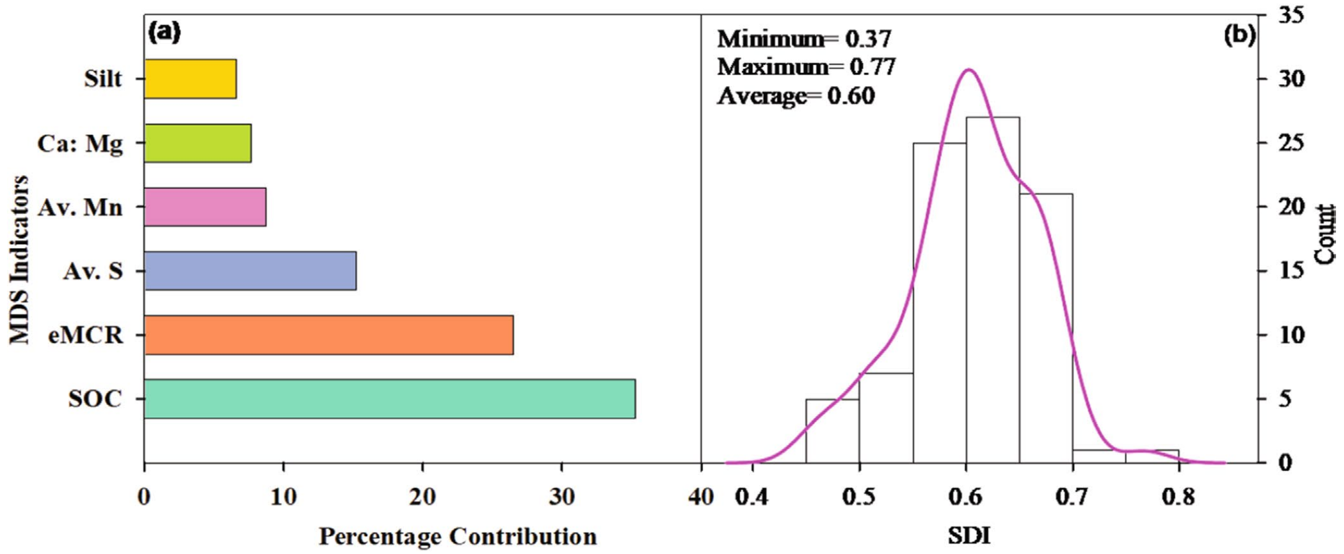

FIGURE 5 | (a) Contribution of MDS indicators for SDI computation; (b) Kernel density plot of SDI.

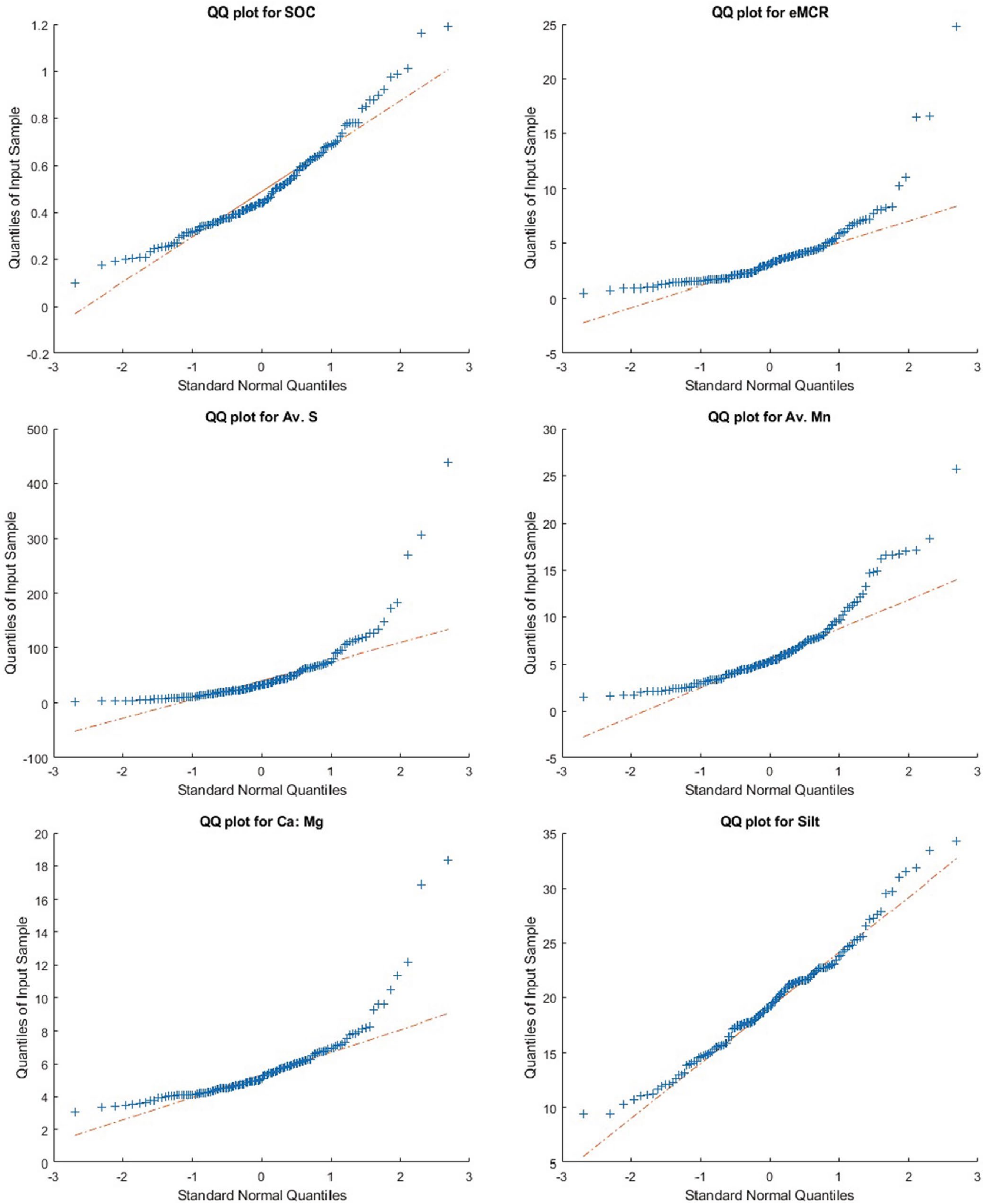

FIGURE 6 | QQ-plots for indicators selected in minimum data set (MDS).

was a strong inverse relationship between SOC content and soil degradation, with SDI values decreasing with increasing SOC contents. The degradation levels associated with SOC content support the assertion that SOC is widely recognised as an indicator of soil degradation (Nascimento et al. 2021; Hancock et al. 2019). This relationship underscores the importance of maintaining or increasing SOC to promote soil health and resilience.

3.3.2 | Reflectance Spectra of Soils and Soil Degradation

Figure 8a shows the typical spectral characteristics of soils collected from areas showing low to high levels of soil degradation in the study area. The highest reflectance was observed at the location with a high SDI value (Figure 8a), while the lowest reflectance was also at a location with a high SDI value, again capturing the decreasing albedo generally seen in soils with increasing SOC contents. These findings align with previous research and provide further evidence of the critical role that SOC plays in soil health and degradation (Nascimento et al. 2021). Figure 8b shows the position of soil samples in the plot between two geometric features (Dufréchou et al. 2015) of water absorption depth at 1900 nm (d_{1900}) and those due to clay minerals around 2200 nm (d_{2200}); most of the soil samples show vermiculitic clay characteristics of vertisols seen in soils originating from basaltic rock systems (Vasava et al. 2019). In addition to these typical absorption features, Figure 8A also shows a strong absorption feature around 900 nm typically observed because of interactions between iron oxides and electromagnetic radiation (Terra et al. 2018).

3.4 | Soil Degradation and Soil Functions

We examined the potential impacts of soil degradation on nutrient retention capacity of soil in the study area (Figure 9) using CEC as an indicator of soil potential to supply nutrients to plants. Although direct measurements of CEC were not available, we utilised a pedo-transfer function to estimate CEC (Rashidi and Seilsepour 2008): CEC = 26.76 + 8.06 × SOC − 2.45 × pH. Results show a strong relationship between estimated SDI and estimated

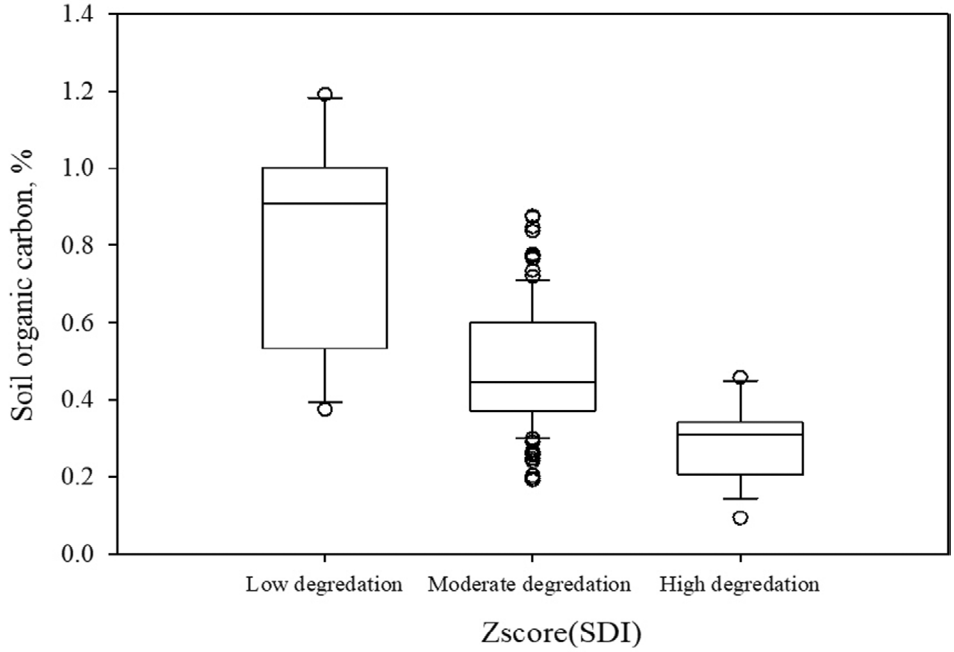

FIGURE 7 | Soil organic carbon at low, medium and high degradation levels.

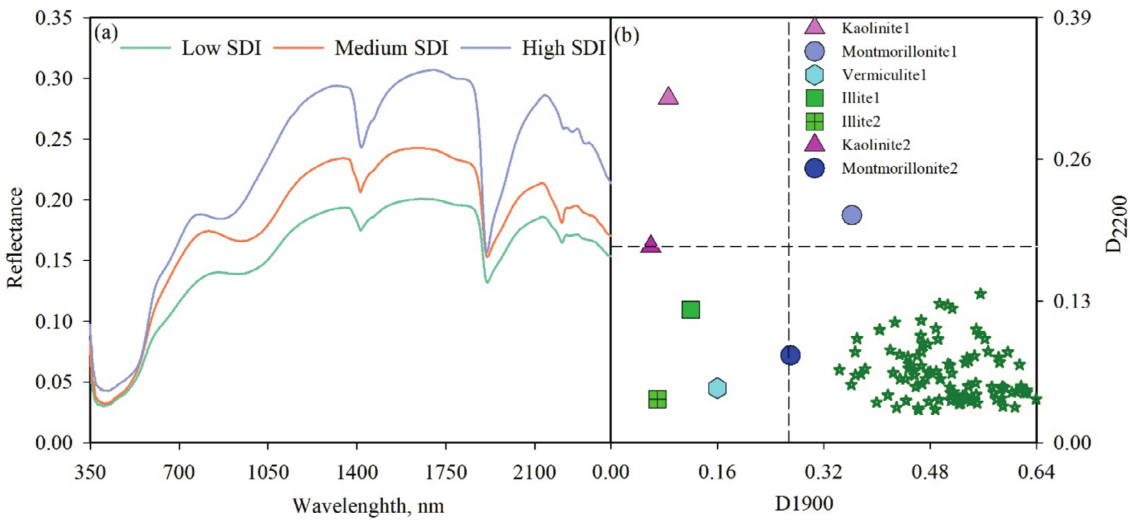

FIGURE 8 | (a) Reflectance spectra of soils at low, medium and high levels of degradation; (b) geometric features of collected soil samples.

CEC values. A significant decline in CEC ($R^2=0.65$) with increasing SDI values reflects the decline in soil nutrient retention capacity with the increased degradation (Figure 9a). This decline highlights the adverse impact of soil degradation on essential soil functions, emphasising the critical need of addressing soil degradation. We further examined the relationship between NDVI and SDI since vegetation can reflect degradation to a certain extent (Wang et al. 2023). The NDVI provides a quantitative measure of vegetation growth and biomass (Wu et al. 2016). On the basis of NDVI values, we first divided the whole study area into five NDVI classes (Figure 9b): 0.0–0.20, 0.20–0.23, 0.23–0.36, 0.36–0.45 and 0.45–0.72. Figure 9b shows the mean SDI value corresponding to each NDVI class. Figure 9b reveals a clear pattern: areas with high vegetation density exhibit lower levels of soil degradation. Conversely, areas with high soil degradation tend to show lower NDVI values, reflecting reduced vegetation growth and biomass. The results highlight the potential of utilising NDVI as a reliable indicator for assessing soil health and guiding sustainable land management practices.

3.5 | Estimation of Soil Degradation Indicators Selected in *MDS* and *SDI* Using Chemometric Modelling

The pre-processing of VIS–NIR spectra was done before carrying out the modelling work. Table 4 shows the performance statistics for estimating soil degradation indicators selected in MDS and integrated SDI with VIS–NIR spectra. Figure 10 shows the observed vs. predicted values of each indicator including SDI obtained using the best modelling approach. Table 4 shows that all SD indicators selected in MDS were predicted with an acceptable accuracy ($R^2>0.6$) except for available S. The SOC content, identified as the primary indicator for degradation, was predicted with R^2 value of 0.82 and RMSE of 0.10% in the validation dataset (Table 4) with SVR as the best prediction model. The results were better than Majeed, Garg, et al. (2023) who obtained an R^2 value of 0.75 in the validation dataset for SOC. The silt content was predicted with R^2 value of 0.69 and RMSE of 2.78%. These results demonstrate better performance than those reported by Vasava et al. (2019) and Viscarra-Rossel et al. (2006) who obtained an R^2 value of 0.55 and 0.52, respectively, for silt content. The eMCR was predicted with an acceptable accuracy with R^2 as high as 0.86 in the validation dataset with $PLSR_{FS}$ as the best prediction model. Other indicators including available S, available Mn and Ca: Mg were also predicted with acceptable accuracy with R^2 values of 0.44, 0.61 and 0.64, respectively. The results show that SDI could be predicted with an R^2 value of 0.81 and RMSE value of 0.03, suggesting that SDI can be estimated using VIS–NIR spectra with an acceptable accuracy. These results suggest that VIS–NIR spectroscopy has the potential in accurately estimating soil degradation indicators.

The study further attempted to estimate SDI with Sentinel-2 L2A data, considering only those sampling locations with high bare soil fractions. This was done by calculating the NDVI values and excluding sampling locations with an NDVI value >0.25. Table 4 shows the performance statistics for estimating SDI with Sentinel-2 L2A data. The results show that SDI can be predicted with an R^2 value of 0.52, an RMSE value of 0.04 and an RPIQ value of 1.81 with SVR as the best prediction model. These results may be considered acceptable given that VIS–NIR spectra obtained an R^2 value of 0.82 and an RMSE of 0.03.

The prediction model built with Sentinel-2 L2A data was applied to each pixel of Sentinel-2 L2A to generate an SDI map for the study area (Figure 11). The results indicate that the major portion of the study area is moderately to highly degraded, with some areas showing low levels of degradation (Figure 11). These maps provide valuable insights to farmers and other stakeholders to identify the hot spots of land degradation and undertake corrective measures. We further examined the relationship between the SDI and yield to understand how soil degradation affects crop productivity (Figure 12). The mapped SDI was correlated with the crop yield of various crops, with rainfed crops including maize and sorghum showing a clear declining trend with the increase in degradation. In contrast,

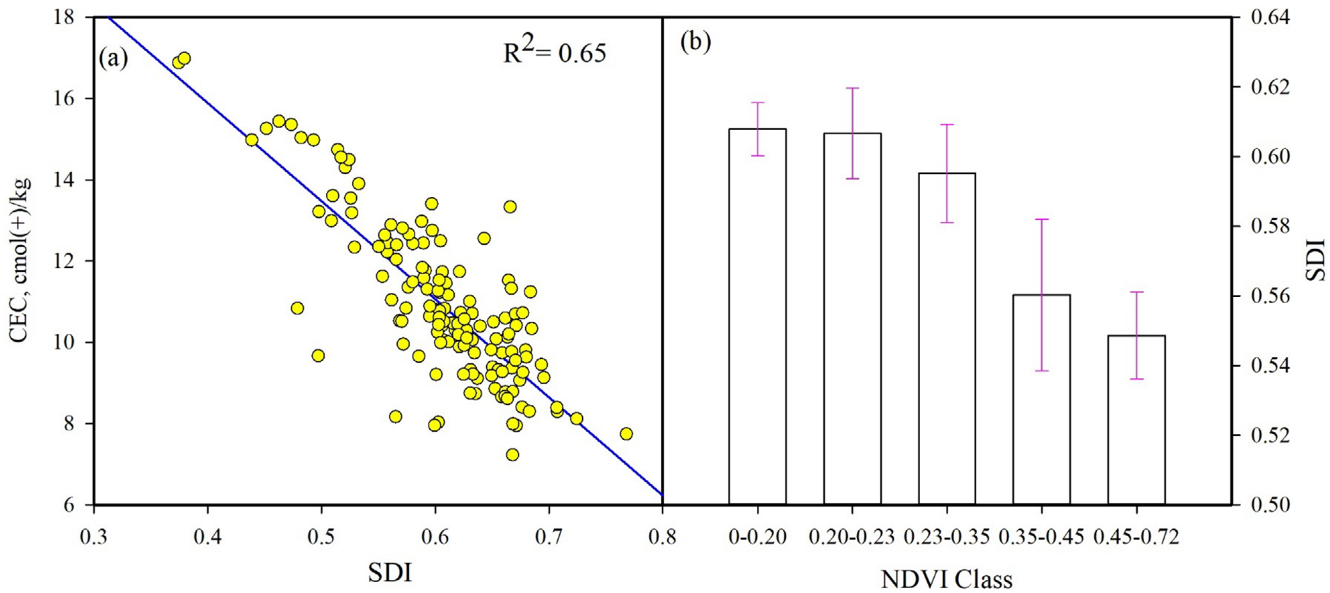

FIGURE 9 | (a) Relationship between SDI and CEC computed with pedo-transfer function; (b) Mean SDI values under each NDVI class.

TABLE 4 | Coefficient of determination (R^2), root-mean-squared error (RMSE) and ratio of performance to interquartile distance (RPIQ) for soil properties selected in minimum data set (MDS) and soil degradation index (SDI) estimated using laboratory spectra and Sentinel-2 L2A data.

Spectral source	Soil indicators	R^2	RMSE	RPIQ	Best model	ST
Laboratory spectra	Silt content	0.69	2.78	2.32	SVR	FD
	SOC content	0.82	0.10	2.39	SVR	UT
	eMCR	0.86	1.19	2.23	$PLSR_{FS}$	SNV
	Av. S	0.44	27.61	1.64	SVR	SNV
	Av. Mn	0.61	2.90	1.66	$PLSR_{FS}$	SNV
	Ca:Mg	0.64	0.80	2.29	SVR	UT
	SDI	0.81	0.03	2.90	SVR	SNV
Sentinel-2 L2A data	SDI	0.52	0.04	1.81	SVR	Log(A)

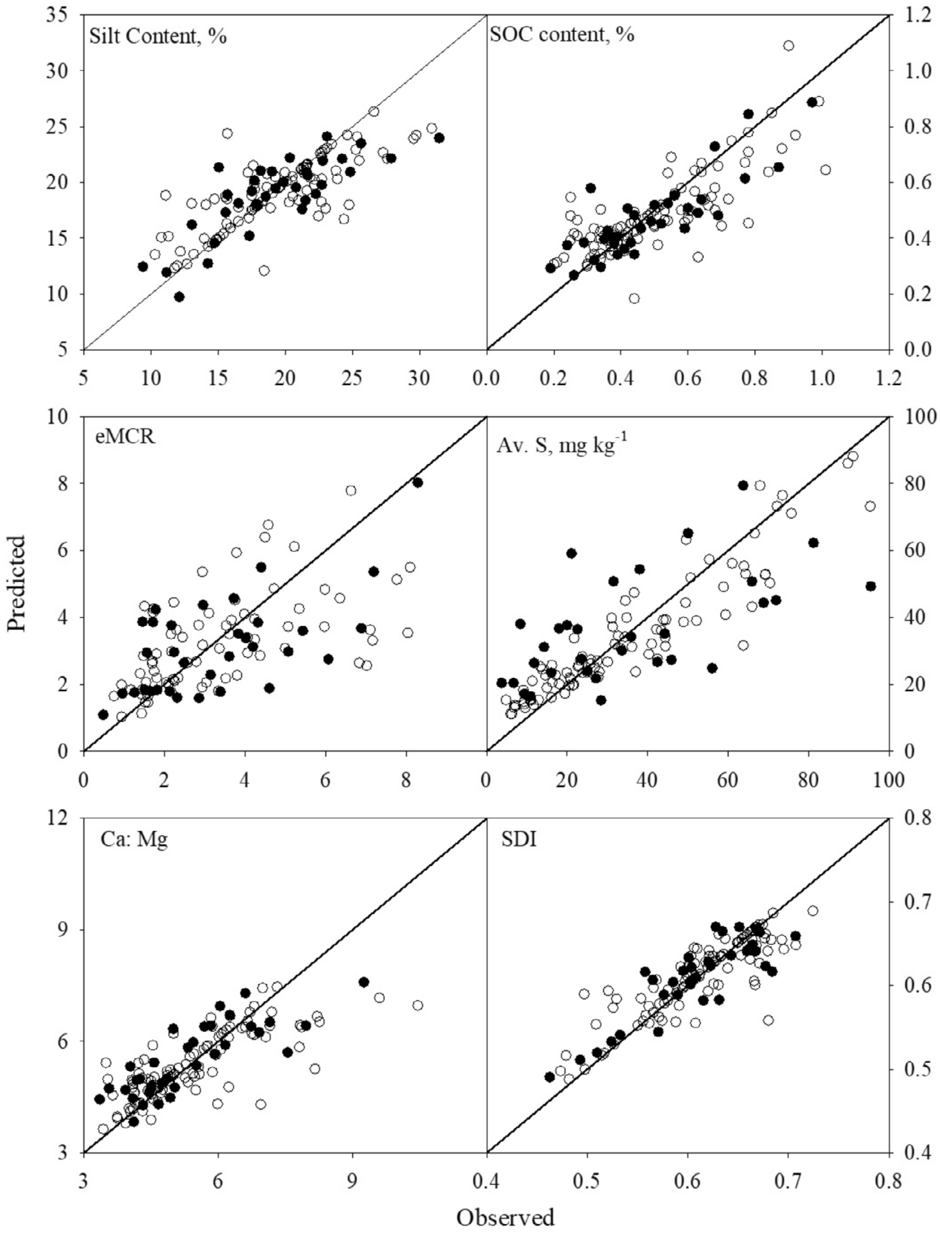

FIGURE 10 | Observed vs. predicted values of soil degradation indicators and soil degradation index (SDI).

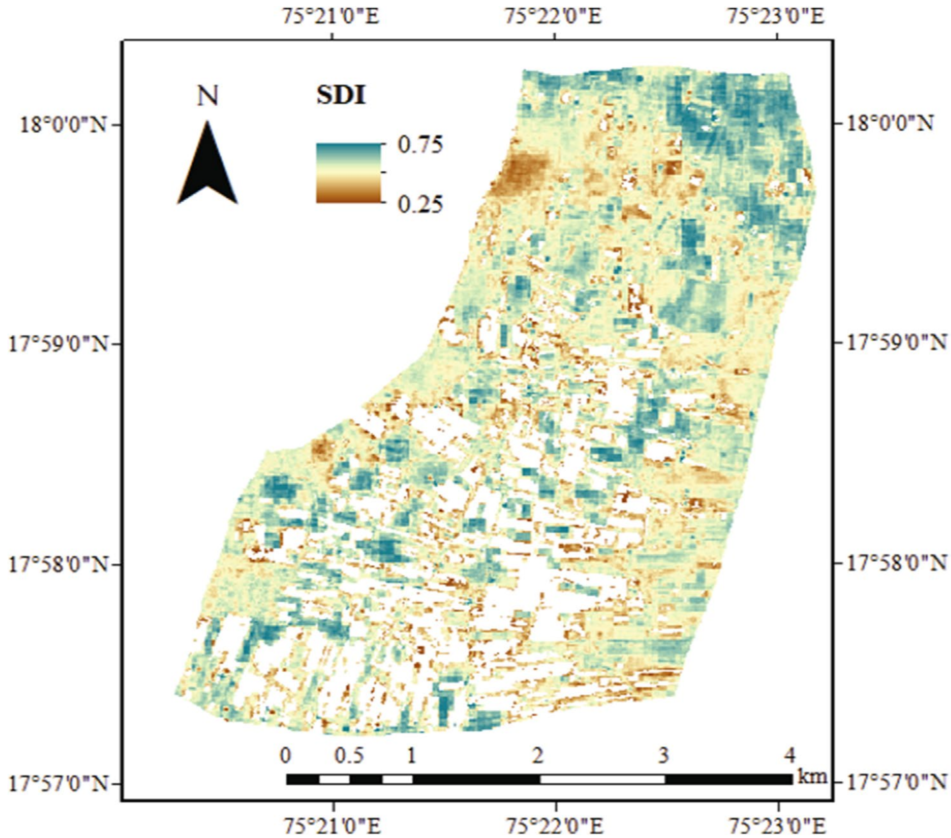

FIGURE 11 | Spatial distribution of SDI across the study area.

the irrigated crops such as onion and sugarcane displayed no consistent trend in response to increasing SDI. This outcome underscores the vulnerability of certain crops to soil degradation, highlighting soil health as a crucial factor in maintaining productivity.

A spatial comparison between SDI and crop yield showed that areas with low crop yield coincided with areas with high SDI values (Figure 13). This spatial association suggests that soil degradation is a key limiting factor influencing crop productivity. The observed pattern reinforces the relevance of SDI as a diagnostic tool for identifying vulnerable agricultural zones requiring targeted management interventions.

4 | Discussion

4.1 | Soil Degradation Index

Soil degradation impacts the soil's ability to perform essential functions, which are vital for agricultural productivity and ecological health. Addressing soil degradation in drylands is crucial for achieving sustainable development goals and mitigating food security threats. The current study identified six parameters- SOC, eMCR, available S, available Mn, Ca: Mg and silt content are key for constructing SDI. Measuring all the physical and nutrient parameters would be complex and expensive. In the current study, SDI values demonstrated a strong relationship with crop yields particularly crops those are cultivated under a rainfed condition. The results also demonstrate the significant impact of soil degradation on CEC. As soil degradation progresses, there is a marked decline in CEC, indicating a reduced ability of the soil to hold essential nutrients and cations. Consequently, the soil's fertility is compromised, affecting plant growth and productivity. In addition, a strong relationship was observed between SOC and SDI, indicating higher SOC content is associated with reduced soil degradation. The study clearly indicated that SDI could be an initial indicator to map soil degradation levels at the field to landscape scale.

4.2 | Laboratory and Remote Sensing-Based Spectroscopy to Quantify Soil Degradation

The proximal- and remote sensing-based DRS offers an opportunity to estimate soil composite parameters such as SDI. Limited efforts have been made to estimate SDI with VIS–NIR laboratory- and remote sensing-based reflectance data. The results obtained in this study show promise for estimating SDI using VIS–NIR laboratory- and remote sensing-based reflectance data. The R^2 values obtained from VIS–NIR spectra indicate that controlled, high-resolution spectral data can effectively predict SDI ($R^2 > 0.8$) and degradation indicators ($R^2 > 0.6$). The results obtained with Sentinel-2 L2A data show promise with SDI predicted with an RMSE value of 0.04. These results suggest that DRS in the proximal and remote sensing mode can serve as a cost-effective alternative for large-scale monitoring of soil degradation, reducing and complementing the time-consuming traditional laboratory methods.

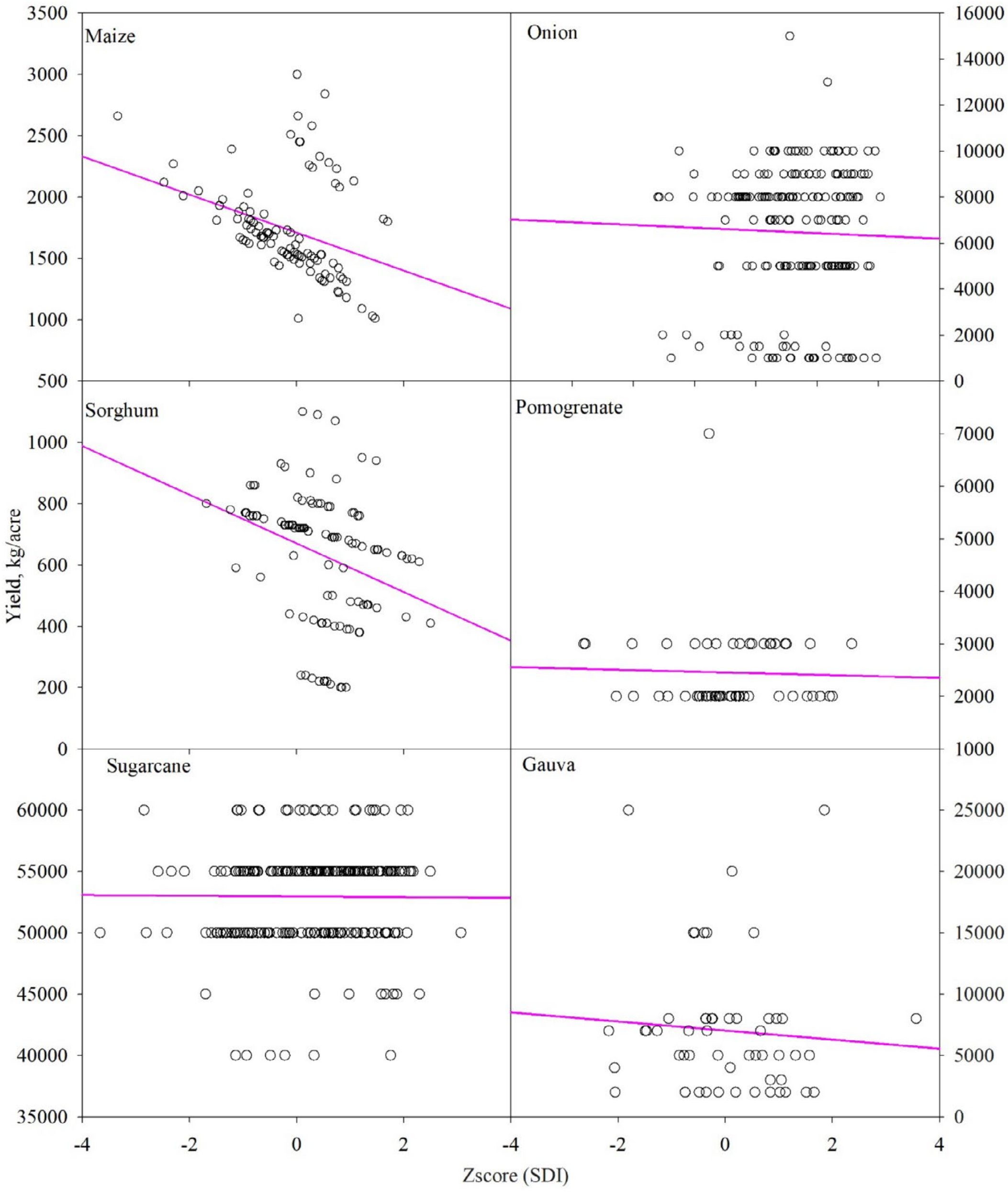

FIGURE 12 | Relationship between soil degradation and yield for rainfed and irrigated crops.

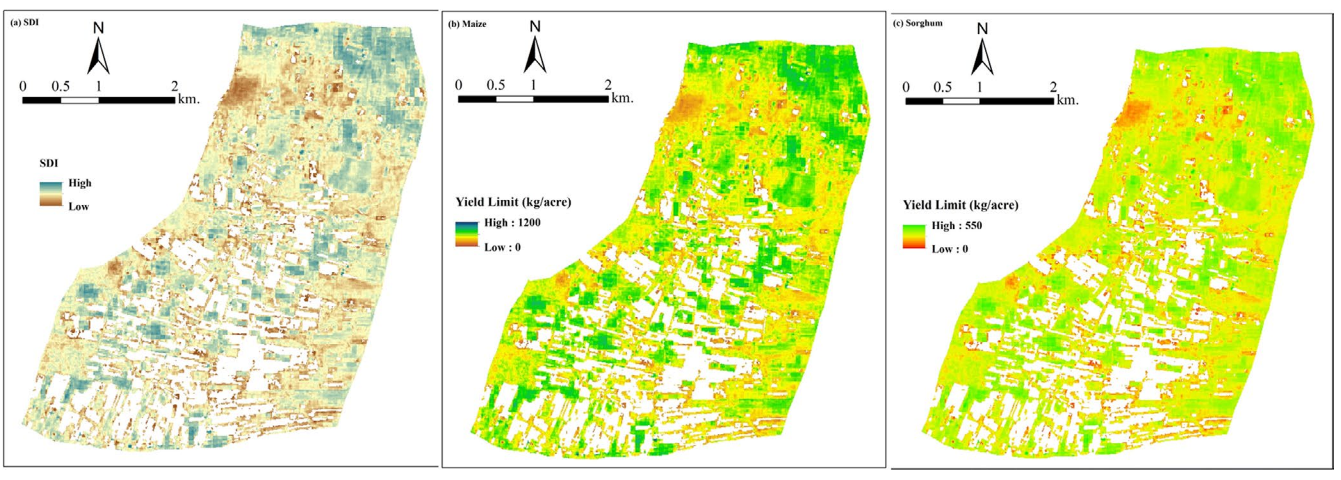

FIGURE 13 | Spatial comparison between (a) Soil Degradation Index (SDI), (b) maize yield limit and (c) sorghum yield limit.

4.3 | Mapping of Soil Degradation for Combating Desertification

In drylands, where water scarcity and extreme weather conditions challenge farming, the additional burden of degraded soils drastically increases fertiliser use and the cost of cultivation. Therefore, mapping of soil degradation is crucial for understanding the hotspots and judicious use of available natural resources for sustaining agricultural yields and ensuring food security. The significance of this study lies in its potential to improve the efficiency and accuracy of soil degradation assessment using advanced science tools. By employing spectroscopy-based technologies, it is possible to overcome the limitations of traditional methods and obtain more comprehensive data on soil health. The approach employed in this can be used to identify hotspots of degradation where immediate action is needed, as well as areas that are still relatively intact but at risk of degradation if current land use practices continue. With this information, specific interventions to tackle soil degradation can be developed, hence addressing its possible impact on soil function and low crop yields. The findings of this research also align with global efforts in soil degradation management including the United Nations Convention to Combat Desertification (UNCCD) and the Sustainable Development Goals (SDGs).

Building on the results of this study, future research could explore the integration of multispectral data with other remote sensing platforms that offer contiguous information such as hyperspectral imaging data. The availability of hyperspectral data from AVRIS-NG and PRISMA sensors may potentially improve the predictions of identified soil degradation indicators as well as SDI and enhance soil degradation processes that are less visible with multispectral data. The fusion of these data sources could result in a more accurate prediction of SDI maps, enhancing our understanding of monitoring soil degradation in real time.

5 | Conclusion

At the current level of science advances, the DRS approach over the proximal and remote sensing mode may be used to overcome the challenge of estimating SDI with traditional methods. This study highlights the potential of the DRS approach as a tool for assessing soil degradation in an agricultural landscape both in the proximal and remote sensing mode. The prediction accuracy obtained for SDI using laboratory spectra ($R^2=0.81$) and Sentinel-2 L2A data ($R^2=0.52$) confirms the potential of DRS in capturing the extent of soil degradation for a large geographical area with the possibility to monitor soil degradation with minimum ground survey (reducing frequent field visits). Specifically, the ability to monitor soil degradation using Sentinel-2 L2A data allows for a temporal assessment of SDI for large areas provided bare soil and clear sky conditions prevail. The calibrated model applied to the Sentinel-2 L2A imagery to map SDI for the entire study area revealed degradation trends that closely aligned with yield variations in rainfed crops. Areas with irrigated crops did not show any consistent effect of degradation on yield, suggesting that management measures may be effectively used for tackling soil degradation. Thus, the current study presents a scalable approach for soil degradation assessment in semi-arid agricultural landscapes, making it accessible and implementable in regions where conventional monitoring is limited by time, resources and spatial limitations. In our study, we estimated SDI values using Sentinel-2 L2A data only for locations that have NDVI values below 0.4. Thus, a specific limitation in our study is that the developed SDI model is applicable only to bare soil conditions. As a future scope of our study, we envision that the SDI values may still be estimated for variably vegetated conditions if hyperspectral remote sensing data are available for unmixing to obtain soil spectra.

Acknowledgements

The authors gratefully acknowledge the funding support received from Groundwater Survey and Development Agency Government of Maharashtra under the Atal Bhujal Yojana for establishing seven benchmarking sites during 2023–2026. Support of CGIAR- science program of Multifunctional Landscape (MFL) is also acknowledged for partially covering ICRISAT scientists' time for undertaking this study. Authors are also thankful to the field and laboratory staff for their meticulous efforts in collecting soil samples and their analysis.

Conflicts of Interest

The authors declare no conflicts of interest.

Data Availability Statement

The data that support the findings of this study are available from the corresponding author upon reasonable request.

References

Adeniyi, S. A., W. P. De Clercq, and A. Van Niekerk. 2017. "Development of a Composite Soil Degradation Assessment Index for Cocoa Agroecosystems in Southwestern Nigeria." *Solid Earth* 8, no. 4: 827–843.

Andrews, S. S., and C. R. Carroll. 2001. "Designing a Soil Quality Assessment Tool for Sustainable Agroecosystem Management." *Ecological Applications* 11, no. 6: 1573–1585.

Andrews, S. S., D. L. Karlen, and J. P. Mitchell. 2002. "A Comparison of Soil Quality Indexing Methods for Vegetable Production Systems in Northern California." *Agriculture, Ecosystems & Environment* 90, no. 1: 25–45.

Awoonor, J. K., E. E. Amoako, B. F. Dogbey, and I. Wiredu. 2024. "Quantitative Analysis of Soil Degradation in Response to Land Use Change in the Guinea Savanna Zone of Ghana." *Geoderma Regional* 37: e00779.

Bhattacharyya, T., D. K. Pal, C. Mandal, et al. 2013. "Soils of India: Historical Perspective, Classification and Recent Advances." *Current Science* 104: 1308–1323.

Birajdar, F., and M. Shaikh. 2024. "Groundwater Exploration and Assessment in Arid and Semi-Arid Regions of Basaltic Terrain of Solapur: Lessons Learned and Future Prospects." *International Journal of Innovative Science and Research Technology* 9: IJISRT24APR2344.

Brady, N. C., and R. R. Weil. 2008. *The Nature and Properties of Soil*. 13th ed. Prentice Hell.

Castaldi, F. 2021. "Sentinel-2 and Landsat-8 Multi-Temporal Series to Estimate Topsoil Properties on Croplands." *Remote Sensing* 13, no. 17: 3345.

Castaldi, F., A. Hueni, S. Chabrillat, et al. 2019. "Evaluating the Capability of the Sentinel 2 Data for Soil Organic Carbon Prediction in Croplands." *ISPRS Journal of Photogrammetry and Remote Sensing* 147: 267–282.

Castaldi, F., M. H. Koparan, J. Wetterlind, et al. 2023. "Assessing the Capability of Sentinel-2 Time-Series to Estimate Soil Organic Carbon and Clay Content at Local Scale in Croplands." *ISPRS Journal of Photogrammetry and Remote Sensing* 199: 40–60.

Dalal, R. C., and S. Jayaraman. 2025. "Nature of Fertility Degradation." In *Soil Fertility Degradation, and Soil Health Restoration and Management*, 65–126. Springer Nature Singapore.

de Sousa Mendes, W., J. A. Demattê, M. E. B. de Resende, et al. 2022. "A Remote Sensing Framework to Map Potential Toxic Elements in Agricultural Soils in the Humid Tropics." *Environmental Pollution* 292: 118397.

Delelegn, Y. T., W. Purahong, A. Blazevic, et al. 2017. "Changes in Land Use Alter Soil Quality and Aggregate Stability in the Highlands of Northern Ethiopia." *Scientific Reports* 7, no. 1: 13602.

Deshpande, S. B., L. R. Hirekerur, R. S. Murthy, and Indian Council of Agricultural Research. 1981. *Benchmark Soils of India—Morphology, Characteristics, and Classification for Resource Management*. National Bureau of Soil Survey and Land Use Planning.

Dufréchou, G., G. Grandjean, and A. Bourguignon. 2015. "Geometrical Analysis of Laboratory Soil Spectra in the Short-Wave Infrared Domain: Clay Composition and Estimation of the Swelling Potential." *Geoderma* 243: 92–107.

Dvorakova, K., U. Heiden, K. Pepers, G. Staats, G. van Os, and B. van Wesemael. 2023. "Improving Soil Organic Carbon Predictions From a Sentinel–2 Soil Composite by Assessing Surface Conditions and Uncertainties." *Geoderma* 429: 116128.

FAO, F. 2020. "Food and Agriculture Organization of the United Nations." Rome. http://faostat.fao.org.

Garg, K. K., K. H. Anantha, M. L. Jat, et al. 2024. "Drought Management in Soils of the Semi-Arid Tropics." In *Managing Soil Drought*, 161–211. CRC Press. https://doi.org/10.1201/b23132-6.

Gee, G. W., J. W. Bauder, and A. Klute. 1986. *Methods of Soil Analysis, Part 1, Physical and Mineralogical Methods*, 5. Soil Science Society of America, American Society of Agronomy.

Gómez, J. A., S. Álvarez, and M. A. Soriano. 2009. "Development of a Soil Degradation Assessment Tool for Organic Olive Groves in Southern Spain." *Catena* 79, no. 1: 9–17.

Gozukara, G., M. Acar, E. Ozlu, O. Dengiz, A. E. Hartemink, and Y. Zhang. 2022. "A Soil Quality Index Using vis-NIR and pXRF Spectra of a Soil Profile." *Catena* 211: 105954.

Guo, L., X. Sun, P. Fu, et al. 2021. "Mapping Soil Organic Carbon Stock by Hyperspectral and Time-Series Multispectral Remote Sensing Images in Low-Relief Agricultural Areas." *Geoderma* 398: 115118.

Hancock, G. R., V. Kunkel, T. Wells, and C. Martinez. 2019. "Soil Organic Carbon and Soil Erosion–Understanding Change at the Large Catchment Scale." *Geoderma* 343: 60–71.

Hanway, J. J., and H. Heidel. 1952. "Soil Analysis Methods as Used in Iowa State College Soil Testing Laboratory." *Iowa Agriculture* 57: 1–31.

Havlin, J. L., J. D. Beaton, S. L. Tisdale, and W. L. Nelson. 1999. "Potassium." In *Soil Fertility and Fertilizers: An Introduction to Nutrient Management*, edited by J. L. Havlin, J. D. Beaton, S. L. Tisdale, and W. L. Nelson, 6th ed., 14–15. Pearson.

Kaiser, H. F. 1960. "The Application of Electronic Computers to Factor Analysis." *Educational and Psychological Measurement* 20, no. 1: 141–151.

Keren, R. 1996. *"Boron", in Methods of Soil Analysis, Part 3. Chapter 21. Chemical Methods. Soil Science Society of America. Book Series*, edited by D. L. Sparks, 603–623. Soil Science Society of America, American Society of Agronomy. https://doi.org/10.2136/sssabookser5.3.c21.

Klute, A. 1986. "Water Retention: Laboratory Methods." In *Methods of Soil Analysis. Part 1. Physical and Mineralogical Methods*, edited by A. Klute, 635–662. American Society of Agronomy–Soil Science Society of America.

Lal, R. 2015. "Restoring Soil Quality to Mitigate Soil Degradation." *Sustainability* 7, no. 5: 5875–5895.

Lal, R. 2004. "Soil Carbon Sequestration Impacts on Global Climate Change and Food Security." *Science* 304, no. 5677: 1623–1627.

Lal, R., and B. A. Stewart, eds. 2019. *Soil Degradation and Restoration in Africa*. CRC Press.

Leul, Y., M. Assen, S. Damene, and A. Legass. 2023. "Effects of Land Use Types on Soil Quality Dynamics in a Tropical Sub-Humid Ecosystem, Western Ethiopia." *Ecological Indicators* 147: 110024.

Levi, N., A. Karnieli, and T. Paz-Kagan. 2022. "Airborne Imaging Spectroscopy for Assessing Land-Use Effect on Soil Quality in Drylands." *ISPRS Journal of Photogrammetry and Remote Sensing* 186: 34–54.

Majeed, I., and B. S. Das. 2024. "Large-Scale Mapping of Soil Quality Index in Different Land Uses Using Airborne Hyperspectral Data." *IEEE Transactions on Geoscience and Remote Sensing* 62: 1–12.

Majeed, I., K. K. Garg, A. Venkataradha, et al. 2023. "Diffuse Reflectance Spectroscopy (DRS) for Rapid Soil Testing and Soil Quality Assessment in Smallholder Farms." *European Journal of Soil Science* 74, no. 2: e13358.

Majeed, I., N. K. Purushothaman, P. Chakraborty, N. Panigrahi, H. B. Vasava, and B. S. Das. 2023. "Estimation of Soil and Crop Residue Parameters Using AVIRIS-NG Hyperspectral Data." *International Journal of Remote Sensing* 44, no. 6: 2005–2038.

Majeed, I., K. Singh, C. Fidelis, et al. 2024. "Diffuse Reflectance Spectroscopy for Assessing Soil Quality Indicators in Cocoa Production System Validated Using Multi-Year Data." *Soil Use and Management* 40, no. 2: e13077.

Meng, X., Y. Bao, J. Liu, et al. 2020. "Regional Soil Organic Carbon Prediction Model Based on a Discrete Wavelet Analysis of Hyperspectral Satellite Data." *International Journal of Applied Earth Observation and Geoinformation* 89: 102111.

Mzid, N., F. Castaldi, M. Tolomio, S. Pascucci, R. Casa, and S. Pignatti. 2022. "Evaluation of Agricultural Bare Soil Properties Retrieval From Landsat 8, Sentinel-2 and PRISMA Satellite Data." *Remote Sensing* 14, no. 3: 714.

Nascimento, C. M., W. de Sousa Mendes, N. E. Q. Silvero, et al. 2021. "Soil Degradation Index Developed by Multitemporal Remote Sensing Images, Climate Variables, Terrain and Soil Atributes." *Journal of Environmental Management* 277: 111316.

Olaniya, M., P. K. Bora, S. Das, and P. H. Chanu. 2020. "Soil Erodibility Indices Under Different Land Uses in Ri-Bhoi District of Meghalaya (India)." *Scientific Reports* 10, no. 1: 14986.

Olsen, S. R., and L. E. Sommers. 1982. "Phosphorus." In *Methods of Soil Analysis Part 2 Chemical and Microbiological Properties*, edited by A. L. Page, 403–430. American Society of Agronomy, Soil Science Society of America.

Purushothaman, N. K., K. K. Garg, A. Venkataradha, et al. 2024. "Applicability of Calibrated Diffuse Reflectance Spectroscopy Models Across Spatial and Temporal Boundaries." *Geoderma* 449: 117012.

Qi, Y., J. L. Darilek, B. Huang, Y. Zhao, W. Sun, and Z. Gu. 2009. "Evaluating Soil Quality Indices in an Agricultural Region of Jiangsu Province, China." *Geoderma* 149, no. 3–4: 325–334.

Rashidi, M., and M. Seilsepour. 2008. "Modeling of Soil Cation Exchange Capacity Based on Some Soil Physical and Chemical Properties." *ARPN Journal of Agricultural and Biological Science* 3, no. 2: 6–13.

Rossel, R. V., D. J. J. Walvoort, A. B. McBratney, L. J. Janik, and J. O. Skjemstad. 2006. "Visible, Near Infrared, Mid Infrared or Combined

Diffuse Reflectance Spectroscopy for Simultaneous Assessment of Various Soil Properties.” *Geoderma* 131, no. 1–2: 59–75.

Santra, P., R. N. Sahoo, B. S. Das, R. N. Samal, A. K. Pattanaik, and V. K. Gupta. 2009. “Estimation of Soil Hydraulic Properties Using Proximal Spectral Reflectance in Visible, Near-Infrared, and Shortwave-Infrared (VIS–NIR–SWIR) Region.” *Geoderma* 152, no. 3–4: 338–349.

Sarathjith, M. C., B. S. Das, S. P. Wani, and K. L. Sahrawat. 2014. “Dependency Measures for Assessing the Covariation of Spectrally Active and Inactive Soil Properties in Diffuse Reflectance Spectroscopy.” *Soil Science Society of America Journal* 78, no. 5: 1522–1530.

Sarathjith, M. C., B. S. Das, S. P. Wani, and K. L. Sahrawat. 2016. “Variable Indicators for Optimum Wavelength Selection in Diffuse Reflectance Spectroscopy of Soils.” *Geoderma* 267: 1–9.

Savitzky, A., and M. J. Golay. 1964. “Smoothing and Differentiation of Data by Simplified Least Squares Procedures.” *Analytical Chemistry* 36, no. 8: 1627–1639.

Smola, A. J., and B. Schölkopf. 2004. “A Tutorial on Support Vector Regression.” *Statistics and Computing* 14: 199–222.

Song, J., X. Shi, H. Wang, et al. 2024. “Improving Soil Quality Index Prediction by Fusion of vis-NIR and pXRF Spectral Data.” *Geoderma* 447: 116938.

Sun, W., S. Liu, L. Jiang, et al. 2025. “Prediction and Monitoring of Soil pH Using Field Reflectance Spectroscopy and Time-Series Sentinel-2 Remote Sensing Imagery.” *Geomatica* 77, no. 1: 100053.

Swain, S. R., P. Chakraborty, N. Panigrahi, et al. 2021. “Estimation of Soil Texture Using Sentinel-2 Multispectral Imaging Data: An Ensemble Modeling Approach.” *Soil and Tillage Research* 213: 105134.

Tarafdar, P. K., and R. Ray. 2005. “Effect of Trees on Improvement of Physical Environment and Fertility in Soils of West Bengal.” *Bulletin of the National Institute of Ecology* 16: 129–136.

Teofilo, R. F., J. P. A. Martins, and M. M. Ferreira. 2009. “Sorting Variables by Using Informative Vectors as a Strategy for Feature Selection in Multivariate Regression.” *Journal of Chemometrics* 23, no. 1: 32–48.

Terra, F. S., J. A. Demattê, and R. A. V. Rossel. 2018. “Proximal Spectral Sensing in Pedological Assessments: Vis–NIR Spectra for Soil Classification Based on Weathering and Pedogenesis.” *Geoderma* 318: 123–136.

The MathWorks, Inc. 2021. “(R2021b) Matlab.” Natick, Massachusetts: United States.

Vasava, H. B., A. Gupta, R. Arora, and B. S. Das. 2019. “Assessment of Soil Texture From Spectral Reflectance Data of Bulk Soil Samples and Their Dry-Sieved Aggregate Size Fractions.” *Geoderma* 337: 914–926.

Vasu, D., P. Tiwary, and P. Chandran. 2024. “A Novel and Comprehensive Soil Quality Index Integrating Soil Morphological, Physical, Chemical, and Biological Properties.” *Soil and Tillage Research* 244: 106246.

Viscarra Rossel, R. A., T. Behrens, E. Ben-Dor, et al. 2022. “Diffuse Reflectance Spectroscopy for Estimating Soil Properties: A Technology for the 21st Century.” *European Journal of Soil Science* 73, no. 4: e13271.

Viscarra Rossel, R. A., and R. M. Lark. 2009. “Improved Analysis and Modelling of Soil Diffuse Reflectance Spectra Using Wavelets.” *European Journal of Soil Science* 60, no. 3: 453–464.

Walkley, A., and I. A. Black. 1934. “An Examination of the Degtjareff Method for Determining Soil Organic Matter, and a Proposed Modification of the Chromic Acid Titration Method.” *Soil Science* 37, no. 1: 29–38.

Wang, J., J. Peng, H. Li, et al. 2021. “Soil Salinity Mapping Using Machine Learning Algorithms With the Sentinel-2 MSI in Arid Areas, China.” *Remote Sensing* 13, no. 2: 305.

Wang, J., J. Zhen, W. Hu, et al. 2023. “Remote Sensing of Soil Degradation: Progress and Perspective.” *International Soil and Water Conservation Research* 11, no. 3: 429–454.

Wu, Y., W. Li, Q. Wang, et al. 2016. “Landslide Susceptibility Assessment Using Frequency Ratio, Statistical Index and Certainty Factor Models for the Gangu County, China.” *Arabian Journal of Geosciences* 9: 1–16.

Zhang, Y., A. E. Hartemink, J. Huang, and P. A. Townsend. 2021. “Synergistic Use of Hyperspectral Imagery, Sentinel-1 and LiDAR Improves Mapping of Soil Physical and Geochemical Properties at the Farm-Scale.” *European Journal of Soil Science* 72, no. 4: 1690–1717.